Metal artifact reduction in x-ray computed tomography: inpainting versus missing value

Ulrich Heil, *Student Member, IEEE,* Daniel Gross, Ralf Schulze, Ulrich Schwanecke and Elmar Schömer

***Abstract*—A comparison of algorithms for reduction of metal artifacts in x-ray cone beam computed tomography (CBCT) is presented. In the context of algebraic reconstruction techniques (ART) several inpainting algorithms in the image domain are evaluated against missing data strategies. A GPU-based iterative framework is employed for a meaningful comparison of both. Simulation results from an extended Shepp-Logan phantom and real world dental data are given.**

I. Introduction

High-density objects like dental implants, fillings or metal tooth caps produce typical streak artifacts in CBCT. Beam hardening, scatter, noise, exponential edge gradient effect and under-sampling are the main causes of these artifacts [5]. Metal artifact reduction (MAR) strategies concentrate on ignoring or replacing image values because the non-linear attenuated projection data are useless in many cases for reconstruction [11], [9]. Standard projection completion methods often replace the missing values in the sinogram by linear interpolation [7], [9].

Digital image inpainting also termed image interpolation, restoration or completion is a technique to restore the area of a removed object based on the information extracted from the surrounding areas. There are two major methods to proceed: diffusion and transport. For a survey on the mathematical fundamentals, methods, and applications of these approaches see e.g. [4].

In this abstract we compare one appropriate inpainting method [10] with a non-weighted missing value implementation in the field of CBCT and ART.

II. Projection image inpainting

We validated four common non texture image inpainting approaches: a method solving the Navier-Stokes equation [1], Telea's fast single-pass algorithm [10], a variational approach minimizing the total variation [2] and a Wavelet inpainting method [3]. In the following, we concentrate on a diffusion method: the linear, discrete and non iterative thus fast inpainting method by Telea [10]. A disadvantage of this method are unordinary patterns resulting from the inside in traversing. Telea uses the fast marching method to archive an approximation of the distance map of the boundary that enables a fast evaluation.

Manuscript received May 10, 2011. This work was supported by the BMBF (FKZ 1748X09).

U. Heil, D. Gross and U. Schwanecke are with the Department of Design, Computer Science and Media, Hochschule RheinMain, University of Applied Sciences.

R. Schulze is with the Department of Oral Surgery (and Oral Radiology), University Medical Center of the Johannes Gutenberg University Mainz.

E. Schömer, U. Heil and D. Gross are with the Institute for Computer Science, Johannes Gutenberg University Mainz.

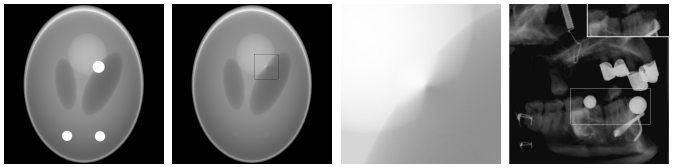

(a) (b) (c) (d)

Fig. 1. X-ray CBCT projection images: (a) the Shepp-Logan artifact phantom and (b) its inpainted counterpart; (c) a detailed view on the image completion of the upper artifact region in (b); (d) a dental projection image supplemented with the inpainted region of interest (compare fig. 3).

III. Missing value implementation

Ignoring missing data is a common method in the field of computed tomography. The projection images or the error sinogram are set to zero at the missing data location [11]. The main linear reconstruction system $\mathbf{Ax} = \mathbf{b}$ can be written as

$$\begin{pmatrix} \mathbf{A_1} \\ 0 \end{pmatrix} \mathbf{x} = \begin{pmatrix} \mathbf{b_1} \\ 0 \end{pmatrix} \text{ with } \mathbf{A} = \begin{pmatrix} \mathbf{A_1} \\ \mathbf{A_2} \end{pmatrix}, \mathbf{b} = \begin{pmatrix} \mathbf{b_1} \\ \mathbf{b_2} \end{pmatrix}$$

by re-sorting all rows in $\mathbf{A}$ with $\mathbf{b_2} = 0$ for missing data. Thereby all equations are ignored by setting $\mathbf{b_2} = 0$ in each iteration. Finally, the predefined artifact mask is added to the reconstruction. Missing value implementations differ from ordinary reconstruction algorithms in applying the missing value mask to the image vector $\mathbf{b}$ in each ART iteration additionally. Since we allow an arbitrary and independent missing value mask for each projection image, the number of equations per voxels x_i varies between $0, \ldots, n$. Fig. 2(d) depicts a typical artifact pattern given by the different number of projections contributing to a voxel. This aspect must be taken into account by a weighted projection and back projection operator.

IV. Results

One inpainting and one missing value method are validated in a comparable and standardized simulation study. The Shepp-Logan phantom [8] is supplemented by three elliptic artifact objects. Its projection images are used together with the priori known artifact mask as input for the evaluated methods (see fig. 1). More precisely all non-zero pixel values from a separate forward projection of the three elliptic artifact objects define the artifact mask.

The reconstructed volumes are compared with the standard Shepp-Logan phantom reconstruction (see fig. 2 and table I). To simulate a comparable realistic scenario with beam hardening we apply a non-linear absorption (NLA) function on the projection values.

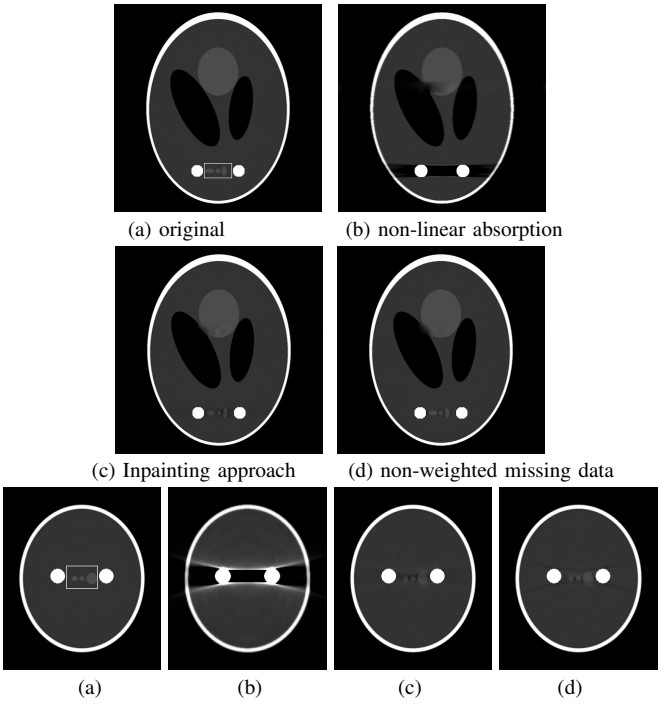

(a) original (b) non-linear absorption

(c) Inpainting approach (d) non-weighted missing data

(a) (b) (c) (d)

Fig. 2. Central slices of the reconstructed, supplemented Shepp-Logan phantom. The relevant region of interest between to artifacts is shown in (a). Further changes from the third artifact source are visible in the dense ellipsoid. The lower row displays a top view onto reconstructed slices between two artifact spheres.

We use a GPU based implementation of the projected Landweber method onto convex subsets to ensure positivity [6]. Subsequently, we set the artifact regions in fig. 2 to the maximum density value for all reconstructions. Here, the missing value approach delivers null and inpainting misleading densities of any order. This regions must be omitted and replaced in the results anyway. Telea's algorithm and the missing value approach give approximately equivalent results (see table I).In fig. 3 reconstructions of a real dental patient dataset with many gold caps and two manually added metal ball bearings are shown.

V. Conclusion

At first glance inpainting techniques seem to be a reasonable alternative to the missing value approach in order to restore pixel values in x-ray projection images even in larger regions. They deliver smooth transition to their local neighborhood, which does suppress artifacts and leads to a local loss in resolution. On the other hand in realistic scenarios extrema as boundary conditions could degrade the results dramatically. In contrast the missing value approach is more reliable, but may yield extra artifacts or instabilities in the iterative solving process. Thus, weighting the amount of contributing images reduces artifacts particularly.

Inpainting errors are less predicable due to the applied technique but are visually comparable to missing value errors. So inpainting is an alternative if we take care about stability of ART solvers or have too many independent artifact regions, as e.g. in dental imaging. Adding information about the detector motion or the object relative positions in 3d into inpainting methods could be a promising future task to make inpainting superior to missing value approaches.

	realistic (NLA)	**inpainting**	**missing value**
complete volume (400^3)			
max. diff. density	0.34	0.21	0.30
sum of squared errors	51558	282.1	251.9
incorrect voxels($\epsilon > 0.01$)	2.3 %	0.32 %	0.19 %
region of interest between artifacts ($55 \times 50 \times 100$)			
max. diff. density	1.81	0.12	0.15
sum of squared errors	2091.53	23.03	15.88
incorrect voxels($\epsilon > 0.01$)	50.0 %	9.8 %	6.9 %

TABLE I
COMPACT SIMULATION RESULTS: COMPARISION WITH THE ARTIFACT-FREE RECONSTRUCTION OF THE SHEPP-LOGAN PHANTOM. THE KNOWN ARTIFACT MASK VOXELS ARE EXCLUDED.

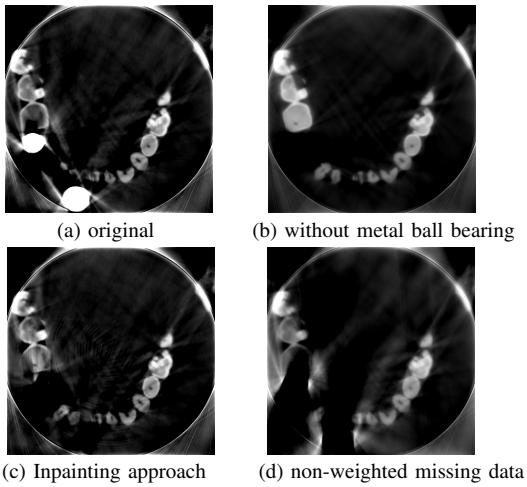

(a) original (b) without metal ball bearing

(c) Inpainting approach (d) non-weighted missing data

Fig. 3. Axial slices through a row of teeth reconstructed with 400^3 from 516 projections with 584x616 pixels and 0.2 mm pixel size of a dry human skull acquired with a 3D Accuitomo (J. Morita Cooperation). The slices display both manually added metal ball bearings shown in fig. 1(d).

References

[1] M. Bertalmio, A. Bertozzi, and G. Sapiro. Navier-Stokes, fluid dynamics, and image and video inpainting. Proc. IEEE Computer Vision and Pattern Recognition(CVPR), Hawaii, 2001.

[2] T. F. Chan and J. Shen. Mathematical models for local deterministic inpaintings. SIAM Journal of Applied Math., 62(3):10191043, 2001.

[3] T. F. Chan, J. Shen and H. M. Zhou. Total variation wavelet inpainting. UCLA CAM report, 04-47, 2004.

[4] T. F. Chan and J. Shen. Image Processing and Analysis: Variational, PDE, Wavelet, and Stochastic Methods. SIAM, Philadelphia, 2005.

[5] B. De Man, J. Nuyts, P. Dupont, G. Marchal and P. Suetens. Metal Streak Artifacts in Xray Computed Tomography: A Simulation Study, IEEE Trans Nucl Sci, vol.46, nr.3, pp.691-696, 1999.

[6] D. Gross, U. Heil, R. Schulze, E. Schömer and U. Schwanecke. GPU-based volume-reconstruction from very few arbitrarily aligned X-ray images. SIAM J Sci Comp 2009; 31: 42044221.

[7] J.-W. Gu, L. Zhang, G.-Q. Yu, Y.-X. Xing and Z.-Q. Chen. X-ray CT metal artifacts reduction through curvature based sinogram inpainting, Journal of X-Ray Science and Technology, 14:2, pp. 73-82, 2006.

[8] A. K. Jain. Fundamentals of Digital Image Processing, Englewood Cliffs, NJ, Prentice Hall, p. 439, 1989.

[9] W. A. Kalender, R. Hebel and J. Ebersberger. Reduction of CT artifacts caused by metallic implants. Radiology, 164(2):576,577, 1987.

[10] A. Telea. An image inpainting technique based on the fast marching method, J. Graphics Tools 9(1), 23-34, 2004.

[11] G. Wang, D. L. Snyder, J. A. O'Sullivan and M. W. Vannier. Iterative Deblurring for CT Metal Artifact Reduction, IEEE Trans Med Imaging, vol.15, pp.657-664, 1996.